ACS chemical biology

Articles

pubs.acs.org/acschemicalbiology

Analysis of the Mechanism of Action of Potent Antibacterial Hetero-tri-organometallic Compounds: A Structurally New Class of Antibiotics

Michaela Wenzel,[†,#] Malay Patra,[⊥,#] Christoph Helmut Rudi Senges,[†] Ingo Ott,[∥] Jennifer Janina Stepanek,[†] Antonio Pinto,[‡,¶] Pascal Prochnow,[†] Cuong Vuong,[§] Sina Langklotz,[†] Nils Metzler-Nolte,*[,‡] and Julia Elisabeth Bandow*[,†]

[†]Biology of Microorganisms and [‡]Bioinorganic Chemistry, Ruhr University Bochum, Bochum, Germany

[§]AiCuris GmbH & Co. KG, Wuppertal, Germany

[∥]Institute of Medicinal and Pharmaceutical Chemistry, Technische Universität Braunschweig, Braunschweig, Germany

Supporting Information

ABSTRACT: Two hetero-tri-organometallic compounds with potent activity against Gram-positive bacteria including multi-resistant *Staphylococcus aureus* (MRSA) were identified. The compounds consist of a peptide nucleic acid backbone with an alkyne side chain, substituted with a cymantrene, a (dipicolyl)$Re(CO)_3$ moiety, and either a ferrocene (FcPNA) or a ruthenocene (RcPNA). Comparative proteomic analysis indicates the bacterial membrane as antibiotic target structure. FcPNA accumulation in the membrane was confirmed by manganese tracing with atomic absorption spectroscopy. Both organometallics disturbed several essential cellular processes taking place at the membrane such as respiration and cell wall biosynthesis, suggesting that the compounds affect membrane architecture. Correlating with enhanced antibacterial activity, oxidative stress was induced only by the ferrocene-substituted compound. The organometallics described here target the cytoplasmic membrane, a clinically proven antibacterial target structure, feature a bactericidal but non-bacteriolytic mode of action and limited cytotoxicity within the limits of solubility. Thus, FcPNA represents a promising lead structure for the development of a new synthetic class of antibiotics.

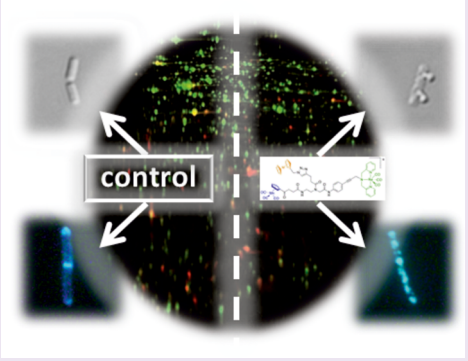

Bacterial antibiotic resistance has become a major public health problem of our time. This is owed to the enormous bacterial adaptability causing rapid resistance development, acquisition, and spread. With a prevalence of methicillin-resistant *S. aureus* (MRSA) in hospitals of up to 50% and the prevalence of multi-resistant Gram-negative pathogens steadily rising, it is clear that new antibiotics with full activity against multi-resistant pathogens are urgently needed. However, the number of newly approved antibiotics steadily declined since the 1980s. Currently, on average less than one antibiotic reaches the market each year.[1] Most of these newly approved antibiotics belong to long-established compound classes and are likely affected by cross-resistance. It is therefore thought that the development of new compounds from old classes is not going to be sufficient to counteract bacterial antibiotic resistance, and the identification of structurally completely new classes is highly desirable.

During the past decade, only three new antibiotic classes were approved for clinical use: cyclic lipopeptides (daptomycin), pleuromutilines (ratapamuline), and glycylcyclines (tigecycline). The glycylcylines are synthetic tetracycline derivatives, thus structurally and mechanistically related to a long established antibiotic class. The cyclic lipopeptides and pleuromutilines are structurally and mechanistically new compounds of microbial origin. Such naturally occurring structures bear the risk of triggering the clinical manifestation of bacterial adaptation strategies long-established in the natural environment of the producer. This has already been observed for daptomycin-resistant strains, which show protective modifications of the cell envelope due to enhanced lipoteichoic acid production.[2,3] In the natural environment, this adaptation of the cell envelope occurs in response to exposure to antimicrobial compounds secreted by other species rendering bacteria cross-resistant to vancomycin and telavancin.[4,5] Fully synthetic structurally novel antibiotic classes might give us an edge in the fight against multi-resistant pathogens by avoiding pre-existing resistance mechanisms.

Recently, we reported a proof-of-principle study on the synthesis of the hetero-tri-organometallic compound FcPNA (Figure 1), attaching three distinct organometallic residues to a building block containing both a peptide nucleic acid (PNA)

Received: February 2, 2013
Accepted: April 11, 2013
Published: April 11, 2013

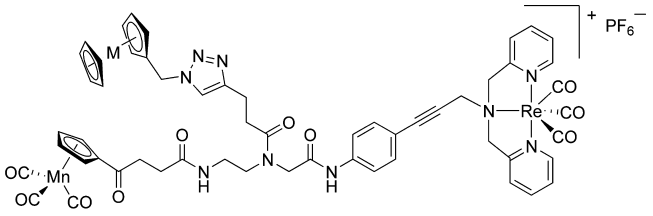

Figure 1. Structures of the hetero-tri-organometallic compounds FcPNA and RcPNA.

backbone and an alkyne side chain.[6] Characterized by a pseudopeptide backbone, a positive charge, and three lipophilic organometallic residues, namely, ferrocene, cymantrene, and a (dipicolyl)Re(CO)$_3$ moiety, FcPNA possesses distinct structural features not occurring in nature. At the same time, it shares chemical properties with membrane-active antimicrobial peptides, which often are both positively charged and lipophilic.[7−9] Here we report on the antibiotic properties of FcPNA and the identification of the bacterial membrane as its antibiotic target structure. We observed an elevation in reactive oxygen species (ROS) *in vivo* in response to FcPNA treatment and were able to link ROS formation to the ferrocene moiety using a ruthenocene-substituted reference compound (RcPNA).

RESULTS AND DISCUSSION

Antibacterial Potency and Cytotoxicity. Antibacterial activity of FcPNA was tested against both Gram-positive and Gram-negative strains according to the Clinical and Laboratory Standards Institute (CLSI) guidelines (Table 1).[10] In water and growth media the limit of solubility was 25 μg mL^{-1}. While within the limit of solubility the organometallic compound was inactive against Gram-negative pathogens (*Pseudomonas aeruginosa*, *Escherichia coli*, *Acinetobacter baumannii*), it exhibited activity against Gram-positive bacteria (*Staphylococcus aureus*, *Bacillus subtilis*) in the low micromolar range comparable to clinically used antibiotics. In contrast to amoxicillin, it exhibited full activity against MRSA strains ATCC 43300 and COL at 2 μg mL^{-1}. FcPNA further showed good activity against the vancomycin-intermediate *S. aureus* (VISA) strain Mu50 at 6 μg mL^{-1}. Survival assays indicated that FcPNA is a bactericidal compound. For *B. subtilis*, the minimal inhibitory concentration of FcPNA equals the minimal bactericidal concentration, achieving more than 5-log reduction in colony forming units after 24 h. Survival rates even 15 min after treatment with 4 μg mL^{-1} FcPNA were reduced to 5% compared to untreated controls. Growth experiments showed that neither compound is bacteriolytic within the limits of solubility (data not shown).

The cytotoxicity of FcPNA against several mammalian cell lines was tested in three different assays (Table 2). Moderate cytotoxicity close to the limit of solubility (around 25 μg mL^{-1}) was observed for NRK-52E and CCRF-CEM cells that were incubated with FcPNA directly after seeding of microtiter plate wells. Variable cytotoxicity was observed when cells were exposed to FcPNA 24 h after seeding, when cells were already attached but still growing into confluency. Under these conditions significant cytotoxicity was observed for MCF7 cells with an IC$_{50}$ of less than 3 μg mL^{-1}, while low cytotoxicity was observed up to the limit of solubility for HepG2 and HT29 cells. Finally, no cytotoxicity was observed against differentiated Caco-2 and L6.C11 cells that were exposed to FcPNA 7 days after seeding, when they were already fully established and no longer growing. All cell lines were grown in the presence of 10% fetal bovine serum. To estimate serum binding of FcPNA, the minimal inhibitory concentration against *B. subtilis* was tested in the presence of 10% bovine serum albumin. A 5-fold increase in the minimal inhibitory concentration was observed in the presence of bovine serum albumin, suggesting that serum binding is approximately 80%.

Table 2. Cytotoxicity of FcPNA against Mammalian Cell Lines at the Limit of Solubility (25 μg mL^{-1}) Determined at Three Different Stages of Growth

cell line	% viability	% SD	IC$_{50}$[a] [μg mL^{-1}]
Caco-2 (human epithelial colorectal adenocarcinoma cell line)[b]	108	12.1	nd
L6.C11 (rat skeletal muscle cell line)[b]	96	14.7	nd
MCF7 (human epithelial breast cancer cell line)[c]	10	2.0	<3
HepG2 (human hepatocellular carcinoma cell line)[c]	92	12.7	nd
HT29 (human colon carcinoma cell line)[c]	83	11.9	nd
NRK-52E (rat kidney epithelial cell line)[d]	55	16.0	nd
CCRF-CEM (human T-cell lymphoblast cell line)[d]	57	6.3	nd

[a]nd: IC$_{50}$ values could not be calculated as 50% inhibition was not reached up to the limit of solubility. [b]Cells were exposed to FcPNA 7 days after seeding. [c]Cells were exposed 24 h after seeding. [d]Cells were exposed directly after seeding.

Table 1. Minimal Inhibitory Concentrations in μg mL^{-1} and μM[a]

	FcPNA		RcPNA		amoxicillin		norfloxacin		vancomycin	
	μg mL^{-1}	μM	μg mL^{-1}	μM	μg mL^{-1}	μM	μg mL^{-1}	μM	μg mL^{-1}	μM
B. subtilis (DSM 402)	2	1.4	32	21	3	8.2	1	3.1	0.5	0.3
S. aureus (DSM 20231)	2	1.4	4	2.7	2	5.5	0.5	1.6	0.5	0.3
S. aureus (ATCC43300) (MRSA)	2	1.4	6	4	48	131	0.5	1.6	1	0.7
S. aureus (COL)(MRSA)	2	1.4								
S. aureus (Mu50) (VISA)	6	4								
E. coli (DSM 30083)	nd	nd	nd	nd	64	175	0.5	1.6	96	66
A. baumannii (DSM 30007)	nd	nd	nd	nd	>256	>700	0.75	2.3	64	44
P. aeruginosa (DSM 50071)	nd	nd	nd	nd	>256	>700	4	13	>512	>353

[a]MIC testing was performed according to Clinical and Laboratory Standards Institute (CLSI) guidelines. Results are reported in the CLSI standard unit for MICs (μg mL^{-1}) and in μM concentration. nd: MIC was not reached up to the limit of solubility (25 μg mL^{-1} for FcPNA and RcPNA).

dx.doi.org/10.1021/cb4000844 | ACS Chem. Biol. 2013, 8, 1442−1450

A ruthenocene analogue, RcPNA (Figure 1), was designed to investigate metal-specific mechanistic differences related to the different redox potentials of ferrocene and ruthenocene (see Supporting Information for synthesis, Supplementary Figures 1−3). Compared to FcPNA, RcPNA displayed lower antibacterial activity (MICs against *B. subtilis* were 2 and 32 μg mL^{-1}, respectively) (Table 1). The small organometallic building blocks of FcPNA and RcPNA by themselves containing a (dipicolyl)Re(CO)3 or cymantrene as well as the ferrocene or ruthenocene carboxylic acids (Supplementary Figure 4) showed no antibacterial activity up to 512 μg mL^{-1}.

Proteomic Profiling. To gain first insights into the antibacterial mode of action of this new class of hetero-tri-organometallics, the response of *B. subtilis* to treatment with FcPNA and RcPNA was investigated by global proteome analyses. Changes in protein synthesis triggered by antibiotic stress often reveal cellular mechanisms of damage control and compensation for loss of function. Over the years, a proteomic response library for the Gram-positive model organism *B. subtilis* has been built that allows the comparison of proteome profiles of structurally new compounds to proteomic profiles of antibacterial agents of known antibiotic classes. Sets of target- or mechanism-specific marker proteins, so-called proteomic signatures, provide a diagnostic tool that can aid in narrowing down the antibiotic target area.[11] As the proteome is highly sensitive to changes in growth conditions, all mechanistic studies were carried out under standardized growth conditions in a chemically defined medium as previously described.[12] Cells were stressed with antibiotic concentrations leading to a significant reduction in growth rates without inflicting lethal damage (Supplementary Figure 5). The FcPNA and RcPNA concentrations required to reduce growth rates of a *B. subtilis* culture growing exponentially in chemically defined medium were similar (2 and 1 μg mL^{-1}, respectively (Supplementary Figure 5)). Proteins newly synthesized in response to the organometallics were then pulse-labeled with L-[^{35}S]-methionine. Cytosolic proteins were subsequently separated by two-dimensional SDS-polyacrylamide gelelectrophoresis, and protein synthesis patterns of antibiotic-treated cells were compared to those of untreated controls.

The proteomic responses to FcPNA and RcPNA treatment were generally very similar (Figure 2). Biosynthesis of many housekeeping proteins was substantially diminished in both cases, evidenced by the majority of protein spots on the 2D gel overlays appearing green, representing proteins no longer synthesized after treatment with the organometallics. FcPNA and RcPNA shared 23 marker proteins (proteins induced more than 2-fold), while 32 markers were unique to FcPNA, and 12 to RcPNA treatment (details on protein function, regulation, and induction factors are provided in Supplementary Tables 1 and 2). Many of the induced marker proteins can be grouped into three related functional categories: cell envelope stress, energy metabolism, and general stress response (Figure 3). Two marker proteins indicative of general cell envelope stress, YceC and YceH,[13] were induced, classifying FcPNA and RcPNA as cell envelope-targeting agents. Moreover, induction of the phage shock protein A (PspA), which stabilizes the membrane by binding to its inner surface, allows narrowing down the antibiotic target to the cell membrane. Upregulation of both PspA and NAD synthase (NadE) suggests that the compounds integrate into the membrane.[13] YoxD, YjdA, and IspH are proteins involved in fatty acid biosynthesis. However, none of the three proteins is part of the standard biosynthetic

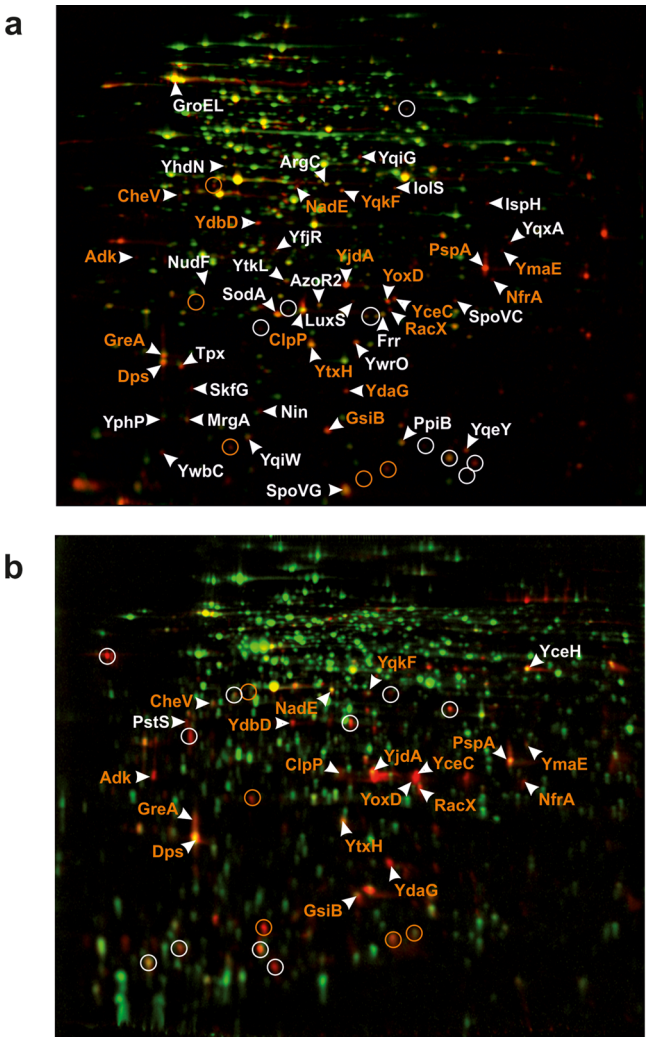

Figure 2. Differential proteome analysis of *B. subtilis* in response to FcPNA and RcPNA. (a) FcPNA, (b) RcPNA. 2D gel-based protein biosynthesis profiles of the controls false-colored in green were overlaid with those of the antibiotic-treated samples false-colored in red. Down-regulated proteins appear green, upregulated proteins red, and proteins expressed at pre-stress rates yellow. Unidentified upregulated proteins are circled. Orange labels indicate proteins induced by both FcPNA and RcPNA, and white labels indicate non-overlapping upregulated proteins.

pathway, suggesting that compound treatment causes a restructuring of the membrane lipid composition. The proteome responses to the organometallics were compared to the antibiotic response library (Supplementary Table 3). Proteins upregulated in response to FcPNA and RcPNA most strongly overlap with marker proteins of potassium carrier ionophore valinomycin and of depolarizing agent gramicidin S (Supplementary Figure 6). In addition to the cell envelope stress response, some of the overlapping proteins were involved in energy metabolism, a further common characteristic for membrane-targeting antibiotics. NadE falls into this category of indicators for energy limitation.[13] Other proteins involved in energy metabolism were also upregulated, particularly by FcPNA, most of which, however, are poorly characterized with regard to their functions. Many of the upregulated proteins are known to participate in the σ^B-dependent general stress response or in sporulation, two alternative strategies of *B. subtilis* for coping with energy limitation.[14] Comparing the

dx.doi.org/10.1021/cb4000844 | *ACS Chem. Biol.* 2013, 8, 1442−1450

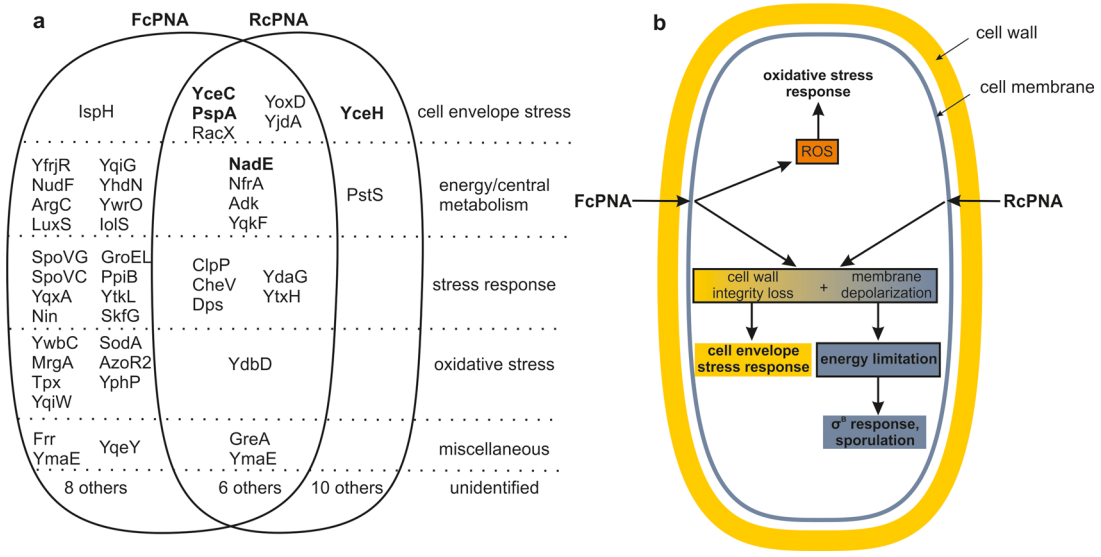

Figure 3. Functional categories of the FcPNA- and RcPNA-induced marker proteins. (a) Overlapping marker proteins of FcPNA and RcPNA. Proteins previously described as markers for general cell envelope and membrane stress are indicated in bold letters. (b) Scheme of the bacterial stress response to the PNA organometallics.

proteome responses to FcPNA and RcPNA treatment, several marker proteins of oxidative stress were upregulated only by the ferrocene but not the ruthenocene-substituted compound, among them metallo-regulated DNA-binding stress protein MrgA and thiol peroxidase Tpx. Both of these stress proteins are regulated in a σ^B-independent fashion. Oxidative stress is also known to trigger the σ^B-dependent general stress response,[15] and we observed that more proteins of the σ^B-regulon were upregulated in response to FcPNA treatment.

Oxidative Stress. CellROX, a fluorescent probe sensitive to reactive oxygen species, was employed to test for intracellular oxidative stress (Figure 4a,b). Paraquat, which causes superoxide formation, served as positive control and led to *B. subtilis* cells fluorescing red. Similarly, red fluorescence was observed after treatment with FcPNA indicating oxidative stress. In contrast, RcPNA-treated cells and untreated controls did not give a fluorescence signal. We conclude that the iron in the ferrocene moiety is redox-active under physiological conditions, probably resulting in the generation of a ferrocene/ferrocenium redox pair that *in vivo* generates reactive oxygen species as part of its redox cycle. However, ferrocene by itself does not seem to be sufficient for antibacterial activity as the ferrocene carboxylic acid building block used to synthesize FcPNA did not show any antibacterial activity (Supplementary Figure 4). As in MIC tests FcPNA showed higher antibacterial potency than RcPNA, it is tempting to speculate that, while it is not essential for bactericidal activity, the oxidative stress component can enhance antibiotic potency.

Influence on Membrane Function. The proteome response to both FcPNA and RcPNA showed upregulation of typical marker proteins for membrane stress. As a Gram-positive bacterium, *B. subtilis* possesses only one membrane, the cytoplasmic membrane, constituting a phospholipid bilayer rich in proteins. To investigate whether FcPNA interacts with the bacterial membrane, its subcellular localization was determined by tracing manganese using atomic absorption spectrometry (AAS). We expect the manganese-containing moiety of FcPNA to be stable under physiological conditions based on previous imaging studies with a compound containing the same manganese–carbonyl building block.[16] Antibiotic-treated cells

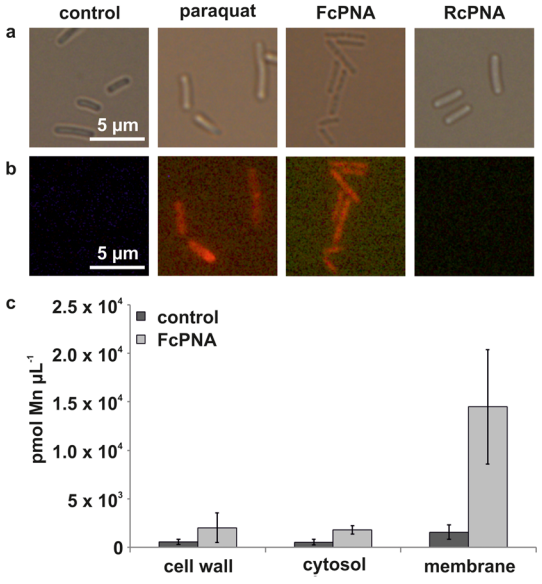

Figure 4. Metal-dependent oxidative stress formation and subcellular localization of FcPNA. (a) Light microscopy and (b) fluorescence microscopy images of CellROX-stained *B. subtilis* cells treated with antibiotics or left untreated demonstrate oxidative stress after FcPNA treatment. (c) FcPNA subcellular localization was investigated by measuring the manganese content of the different cell fractions by atomic absorption spectroscopy. The manganese concentrations in the cell wall, the cytosol, and the membrane were calculated.

were fractionated by differential centrifugation, and the manganese content was determined in the cytosolic, the membrane, and the cell wall fractions (Figure 4c). After treatment with FcPNA, the concentration of manganese in the membrane fraction was about 10-fold higher than in untreated controls and about 6-fold higher than in the cytosolic and cell wall fractions, demonstrating that a majority of FcPNA localizes in or at the *B. subtilis* membrane (Supplementary Figure 7). During sample preparation, cells were repeatedly washed with Tris/EDTA buffer to remove loosely bound manganese. FcPNA seems to bind to the bacterial membrane very tightly

dx.doi.org/10.1021/cb4000844 | ACS Chem. Biol. 2013, 8, 1442–1450

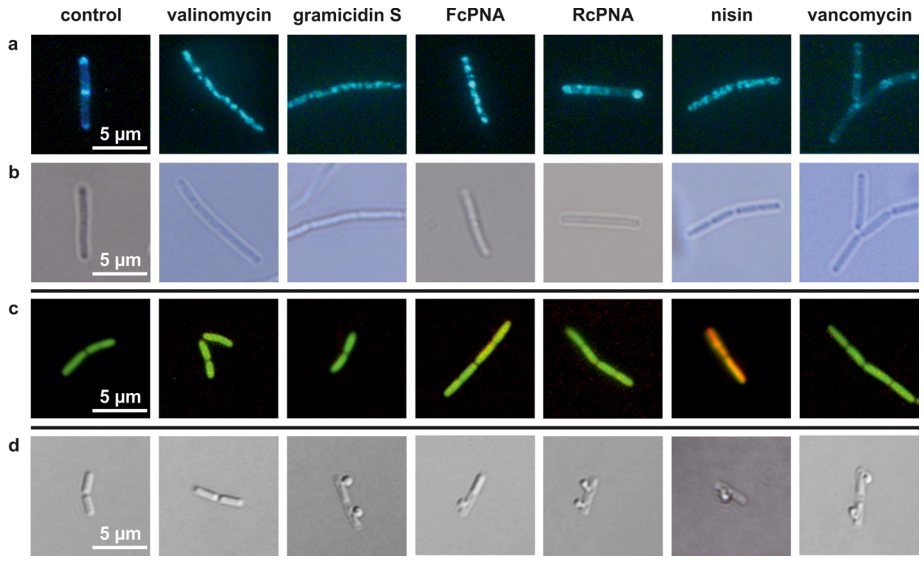

Figure 5. Influence of FcPNA and RcPNA on the *B. subtilis* membrane and cell wall integrity. (a) GFP-MinD localization after antibiotic treatment. (b) Light microscopy images corresponding to panel a. (c) Light microscopy images of antibiotic-treated cells stained with BacLight green dye passing through intact membranes and red dye passing through membrane pores. (d) Antibiotic-stressed cells fixed with acetic acid/methanol.

as little manganese was removed by the washing steps. At the same time, as manganese levels in the cytosol and cell wall fractions increased only slightly after FcPNA treatment, it is unlikely that FcPNA targets cell wall or cytosolic components.

The overlap of marker proteins between the organometallics and valinomycin and gramicidin S suggests that the organometallics might also cause disruption of the cellular membrane potential. Membrane depolarization was monitored using an assay that utilizes the membrane potential-dependent localization of cell division protein MinD. If the membrane potential is intact, MinD localizes at the cell poles and the cell division plane, while upon depolarization MinD delocalizes and distributes irregularly throughout the cell.[13,17] Using a GFP-MinD fusion strain, MinD localization was monitored by fluorescence microscopy (Figure 5a,b). The untreated control as well as vancomycin, an inhibitor of cell wall biosynthesis that does not affect the membrane potential, displayed normal MinD localization. Like valinomycin and gramicidin S, FcPNA and RcPNA led to MinD delocalization, demonstrating membrane depolarization by both organometallics.

Membrane depolarization can be the result of a number of different challenges ranging from inhibition of the respiratory chain to an enhanced bilayer permeability, e.g., due to pore formation or potassium or proton translocation. Using a pair of fluorescent dyes we investigated the potential of FcPNA and RcPNA to form pores. The commercially available BacLight staining kit combines a green-fluorescent dye that readily crosses intact membranes and a red-fluorescent dye, which can only enter bacterial cells through pores in the membrane (Figure 5c). Only nisin, a pore-forming lantibiotic serving as positive control, permeabilized *B. subtilis* for the red dye, resulting in cells fluorescing both red and green. Cells not treated with antibacterial agents as well as cells treated with non-pore-forming comparator compounds fluoresced only green. Since the organometallics fluoresced green, formation of large pores can be excluded as a mechanism of both FcPNA and RcPNA.

Energy Limitation. To examine if the interaction of FcPNA and RcPNA with the membrane causes energy limitation in the cell as suggested by the proteome response, we determined cytosolic ATP levels after treatment with the organometallics (Figure 6). Compared to the untreated control,

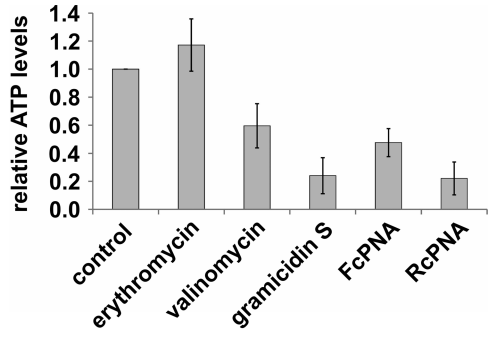

Figure 6. Relative intracellular ATP levels of *B. subtilis* after treatment with FcPNA, RcPNA, and comparator compounds.

valinomycin, a potassium ionophore, and gramicidin S, which was previously shown to permeabilize the membrane for potassium,[18] reduced the ATP content by 40% and 80%, respectively. In contrast, protein biosynthesis inhibitor erythromycin did not influence intracellular ATP levels. FcPNA reduced the cellular ATP content by 50%, demonstrating a strong impact of the organometallic on cellular energy metabolism. The effect on cellular energy levels, however, does not seem to correlate strictly with antibacterial activity, as the less potent RcPNA applied at only 0.66 μM led to ATP levels only half of those observed after treatment with 1.4 μM FcPNA. A decrease in ATP levels after treatment with the organometallics could be a result of membrane depolarization and subsequent cessation of ATP production. However, it could also be an effect of the organometallic compounds on ATP synthase or the respiratory chain, both of which are located at the cytoplasmic membrane.

Cell Wall Integrity. Due to the upregulation of the proteins YceC and YoxD, which were also found to be upregulated by cell wall biosynthesis inhibitors like vancomycin (Supplementary Table 3), we examined the impact of FcPNA and RcPNA on cell wall integrity. If cell wall biosynthesis is inhibited,

dx.doi.org/10.1021/cb4000844 | *ACS Chem. Biol.* 2013, 8, 1442–1450

fixation of antibiotic-treated cells in a 1:3 mixture of acetic acid and methanol leads to deformation of cells.[19] A characteristic formation of membrane extrusions after acetic acid/methanol fixation is typically observed, if a membrane-associated cell wall biosynthesis step is inhibited. This form of membrane blebbing was observed, for instance, after treatment with lipid II-binding compounds nisin and vancomycin, which served as positive controls here (Figure 5d). Both organometallic compounds showed the same aberration in cell shape after acetic acid/methanol fixation, suggesting that FcPNA and RcPNA either directly or indirectly interfere with the cell wall biosynthesis machinery. A direct inhibition of cell wall biosynthesis components by the organometallics is unlikely as the proteome responses to both compounds lack the typical marker proteins for cell wall biosynthesis inhibition, LiaH, YtrE, and YtrB.[13] A similar effect was observed for gramicidin S, which integrates into the bacterial membrane and acts rapidly depolarizing.[13,16] Both gramicidin S and the organometallics might indirectly affect cell wall biosynthesis by disturbing membrane architecture. Despite FcPNA and RcPNA having gramicidin S-like effects on the membrane potential, ATP levels, cell wall integrity, and the proteome, the organometallics differ from gramicidin S in that they are not bacteriolytic.

Conclusion. The recently reported hetero-tri-organometallic compound FcPNA showed potent antibacterial activity against Gram-positive bacteria. It was active against *S. aureus* including MRSA and VISA strains in the low micromolar range, comparable to antibiotics currently used clinically. FcPNA represents a fully synthetic novel class of antibiotics with structures completely new to nature. Generally, aside from antiseptics, organometallics have been underexplored in antibacterial research and development,[20−23] and to our knowledge this work represents the first study on a metal-based antibacterial agent that addresses both the antimicrobial potency and the antibiotic target.

We initiated global proteome-based mechanistic studies to identify the general target area for FcPNA and designed a ruthenocene-substituted derivative, RcPNA, to study metal-specific effects. The proteomic response of *B. subtilis* to the organometallics showed upregulation of marker proteins for cell envelope stress in general and membrane stress in particular. A strong interaction of FcPNA with the cytoplasmic membrane was demonstrated by tracing manganese as a surrogate for the manganese-containing FcPNA using AAS. A direct interaction of FcPNA with the bacterial membrane is consistent with an induction of alternative fatty acid biosynthesis enzymes involved in adjusting the composition of the membrane to antagonize interactions with the organometallics. As shown by fluorescence microscopy, FcPNA and RcPNA efficiently depolarized *B. subtilis* cells. While the cause of depolarization remains to be elucidated, we were able to exclude formation of large pores as a mechanism. Consistent with membrane depolarization, the proteome and a luciferase-based ATP assay revealed severe energy limitation.

An elevation in reactive oxygen species was observed after treatment with FcPNA, but not RcPNA. To our knowledge, we could show here for the first time that ferrocene can induce oxidative stress in a living system. Similar results were previously obtained *in vitro* for the ferrocene-substituted chloroquine-based antimalarial drug candidate ferroquine.[24] Further, Dunbar et al. provided evidence for the colocalization of ferroquine with a sulfur-containing compound, presumably the antioxidant glutathione.[25] Ferroquine provides a rare example of an organometallic compound in clinical development for antimicrobial therapy targeting a unicellular parasite *Plasmodium falciparum*. It has been shown to overcome chloroquine resistance and is about to complete phase II clinical trials.[26] Ferroquine passing phase I clinical trials suggests that there are no major safety issues connected to the ferrocene moiety itself, clearing the way for future ferrocene-containing organometallic drug candidates in the antimicrobial field.

While the molecular mechanism of action of FcPNA remains to be studied further, we were able to identify the cytoplasmic membrane as the target structure. On the basis of the effects observed, we postulate that FcPNA integrates into the phospholipid bilayer causing a change in membrane architecture that affects the function of one or more membrane proteins. However, it is also possible that FcPNA interacts directly with different membrane proteins. The bacterial membrane has been validated as an antibacterial target only in the past decade. As demonstrated by daptomycin, membrane-targeting antibiotics can be successfully applied in the clinic using systemic administration.[27] Membrane-targeting antibiotics were shown to be less prone to bacterial resistance development than antibiotics inhibiting a single enzyme target,[28] making the bacterial membrane a particularly attractive target for future antibiotic development. Based on its potent antibacterial activity and the limited cytotoxicity, FcPNA, representing a novel class of antibiotics, is a promising lead structure that warrants further investigation. The solubility of FcPNA is rather poor and currently prevents systemic administration, thereby limiting evaluation of acute toxicity in animal models. The main goal of future structure−activity relationship studies will be to increase solubility while retaining antibacterial activity and retaining or increasing selectivity for bacteria over mammalian cells.

METHODS

Antibiotics. FcPNA was synthesized as described previously.[5] RcPNA synthesis largely parallels FcPNA synthesis and is described in the Supplementary methods. All antibiotic stock solutions were prepared at 10 mg mL^{-1} in DMSO. Valinomycin and bacitracin were purchased from Sigma-Aldrich. Vancomycin was purchased from Applichem. Gramicidin S was synthesized and purified according to Wadhwani et al.,[29] and nisin was obtained from H.-G. Sahl (University of Bonn, Germany).

Minimal Inhibitory Concentration. Minimal inhibitory concentrations (MIC) were tested against *Escherichia coli* DSM 30083, *Acinetobacter baumannii* DSM 30007, *Pseudomonas aeruginosa* DSM 50071, *Bacillus subtilis* DSM 402, *Staphylococcus aureus* DSM 20231 (type strain), *Staphylococcus aureus* ATCC 43300 and COL (MRSA), and *Staphylococcus aureus* Mu50 (VISA) in a microtiter plate assay according to CLSI guidelines as described previously.[10,30] To estimate serum binding, MIC tests were analogously performed in the presence of 10% bovine serum albumin.

Minimal Bactericidal Concentration. Minimal bactericidal concentration (MBC) against *B. subtilis* 168 was determined in Mueller Hinton medium in a microtiter plate assay. Cells (5×10^5 mL^{-1}) were treated with 1-, 2-, 5-, and 10-fold MIC (2, 4, 10, 20 μg mL^{-1} FcPNA. An untreated control was directly plated on Mueller Hinton agar plates and colony-forming units (CFUs) counted after 16 h of incubation at 37 °C. The antibiotic-treated cultures in the microtiter plates were incubated at 37 °C for 24 h prior to plating of 200 μL of the cultures on Mueller Hinton agar for CFU determination. CFUs were related to those of the untreated control. The antibiotic concentration that led to a CFU reduction of 5 log units was taken as MBC.

Cytotoxicity. Cytotoxiciy against human cancer cell lines was tested in three different assays (for detailed experimental procedures see Supporting Information). Caco-2 and L6.C11 cells were exposed to FcPNA 7 days after seeding when cells had grown into confluency and were fully established and no longer growing. Metabolic activity was determined in a resazurin-based assay. MCF7, HepG2, and HT29 cells were exposed to FcPNA 24 h after seeding, when cells had attached but were still growing into confluency. Viability was determined using a crystal violet-based assay. NRK-52E and CCRF-CEM cells were exposed to FcPNA directly after seeding, and metabolic activity was determined in an Alamar Blue-based assay.

Bacterial Strains and Growth Conditions. For mechanistic studies, *B. subtilis* 168 (*trpC2*)[31] was grown at 37 °C under steady agitation in chemically defined Belitzky Minimal Medium (BMM).[32] In growth experiments, bacterial cultures were treated with different antibiotic concentrations in mid exponential growth phase after reaching an optical density at 500 nm (OD_{500}) of 0.35. For physiological stress experiments, including proteomic studies, antibiotic concentrations were chosen that led to reduced growth rates compared to the untreated control (Supplementary Figure 5).

Determination of Survival Rates. *B. subtilis* was grown in Luria–Bertani (LB) medium at 37 °C under steady agitation to an OD_{500} of 0.35. Five × 10^5 cells per mL were exposed to 4 μg mL^{-1} FcPNA for 15 min or left untreated. Cells were then plated on LB agar plates and incubated overnight before colony forming units were counted. The experiment was performed 4 times independently.

Proteome Analysis. Preparation of radioactively labeled protein extracts and two-dimensional polyacrylamide gelelectrophoresis were performed as described previously.[12] FcPNA was applied at a concentration of 2 μg mL^{-1} (2.9 μM), and RcPNA at 1 μg mL^{-1} (1.5 μM). Proteins were identified by MALDI-ToF/ToF as described previously.[12] Protein spots that could not be identified with this method were identified by nLC–ESI-MS/MS as described in the Supplementary Methods.

Atomic Absorption Spectroscopy. Cells were grown in BMM until early logarithmic growth phase and stressed with 2 μg mL^{-1} (2.9 μM) FcPNA as in the proteomic experiments. After 15 min of antibiotic stress, cells were harvested by centrifugation, washed three times with Tris/EDTA buffer (100 mM Tris/1 mM EDTA, pH 7.5), and disrupted by ultrasonication. Cell debris was kept for measuring the cell wall fraction. The crude cell extract was subjected to ultracentrifugation at 80,000*g* for 4 h. The resulting supernatant yielded the cytosolic fraction. The membrane pellet was dissolved in EDTA-free Tris buffer (100 mM Tris, pH 7.5). Samples were lyophilized using a freeze-dryer BETA I instrument (Martin Christ) at −20 °C overnight. For determination of the manganese content, samples were resuspended in distilled H_2O. Triton X-100 and HNO_3 were added to 200 μL of resuspended samples to final concentrations of 1% and 13%, respectively. Manganese measurements were performed using a ContrAA 700 graphite furnace high resolution continuum source atomic absorption spectrometer (Analytik Jena). Samples were injected at a volume of 20 μL into regular graphite tubes and processed in the furnace according to a recently described protocol.[33] Manganese was detected at a wavelength of 279.4817 nm. The mean absorbance of duplicate injections was used throughout the study. A pure sample of FcPNA was used for calibration. Sensitivities and detection limits of the AAS method depend on the sample matrix and instrument performance. For biological samples measured in this study sensitivities ranged between 0.35–1.12 A μM^{-1} and detection limits reported by the instrument software as characteristic concentrations were in the range of 0.0039–0.0096 μM (1% A)$^{-1}$. Measured manganese concentrations were related to the *B. subtilis* cytosolic, cell wall, and membrane volumes. Volumes of these cell fractions were calculated based on cryo-electron micrographs by Matias and Beveridge.[34,35] The volumes of the cellular cytosolic fraction, the cell wall fraction, and the cell membrane fraction were estimated at 3.09 × 10^{-9} μL, 8.08 × 10^{-10} μL, and 8.99 × 10^{-11} μL, respectively. The experiment was performed three times independently.

Microscopy. All microscopy experiments were performed in three biological replicates. For fluorescence and light microscopy experiments, the following antibiotic concentrations were used to treat *B. subtilis*: 8 μg mL^{-1} (11.6 μM) FcPNA, 6 μg mL^{-1} (8.8 μM) RcPNA, 10 μg mL^{-1} (11.1 μM) valinomycin, 1 μg mL^{-1} (1.1 μM) gramicidin S, 0.75 μg mL^{-1} (2.5 μM) nisin, and 1.5 μg mL^{-1} (2.2 μM) vancomycin. MinD-GFP localization and cell wall integrity were examined as described previously[13] using the *B. subtilis* 1981 GFP-MinD strain[15] obtained from L. Hamoen (Newcastle University, England) or *B. subtilis* 168, respectively.

For the BacLight assay, *B. subtilis* 168 was grown in BMM until reaching mid logarithmic growth phase. The culture was split, and the subcultures were treated with the same antibiotic concentrations described above. After 15 min of antibiotic stress, 2 μL of a 1:1 mixture of the green- and red-fluorescing dyes were added per milliliter of culture volume and incubated for 15 min in the dark under steady agitation. Cells were washed with 100 mM Tris/1 mM EDTA, pH 7.5 and resuspended in the same buffer. Five microliters of the cell suspension was imaged in fluorescent mode as described previously.[13] The Cell Imaging Software was used to merge the green and red channel pictures. The same background value (factor = 25) was subtracted from each single picture.

For the CellROX assay, *B. subtilis* was grown in BMM until early logarithmic growth phase and subsequently divided into subcultures, which were stressed with 25.7 μg mL^{-1} (100 μM) paraquat, 8 μg mL^{-1} (11.6 μM) FcPNA, or 6 μg mL^{-1} (8.8 μM) RcPNA or left untreated as control. After 15 min of antibiotic stress, CellROX Deep Red reagent (Invitrogen) was added, and the cells were incubated for another 30 min. Subsequently, cells were washed in 100 mM Tris/1 mM EDTA and resuspended in the same buffer. Five microliters of cells was imaged without fixation in fluorescence mode using an Olympus BX51 microscope with a U-UCD8 condenser, an UPlanSApo 100XO objective, a U-LH100HGAPO burner, and a U-RFL-T power supply. Pictures were taken using a CC12 digital color camera and the Cell Imaging Software (all components by Olympus).

Determination of Cellular ATP Levels. *B. subtilis* 168 was grown in BMM to an OD_{500} of 0.35 and subsequently exposed to the antibiotics at the same concentrations described above. Erythromycin was applied at 0.5 μg mL^{-1} (0.37 μM). Cells were harvested after 15 min of antibiotic stress by centrifugation, resuspended in 500 μL 10 mM Tris, pH 7.5, and disrupted by ultrasonication as described for proteome analysis. ATP levels were determined using the Perkin-Elmer ATPlite onestep assay kit following the manufacturer's instructions. ATP standards were prepared from 1 × 10^{-7} to 8.5 × 10^{-7} M ATP in the provided buffer. For determination of cellular ATP levels, 100 μL of cytosolic cell extracts was used. All measurements were performed in five independent biological experiments with two technical replicates each using the Tecan Infinite 200 PRO multimode reader (Tecan).

■ ASSOCIATED CONTENT

Ⓢ Supporting Information

This material is available free of charge via the Internet at http://pubs.acs.org.

■ AUTHOR INFORMATION

Corresponding Author

*E-mail: julia.bandow@rub.de; nils.metzler-nolte@rub.de.

Present Addresses

[⊥]Department of Bioinorganic Chemistry, University of Zurich, Switzerland.

[¶]Clinic of Cardiovascular Surgery, Heinrich Heine University Düsseldorf, Germany.

Author Contributions

[#]These authors contributed equally to this work.

Notes

The authors declare no competing financial interest.

■ ACKNOWLEDGMENTS

This work was financially supported by a fellowship of the International Max Planck Research School for Chemical Biology (M.P.), the Research Department *Interfacial Systems Chemistry* at Ruhr University Bochum (N.M.-N., J.E.B.), the DFG (N.M.-N.), and the European Regional Development Fund "Investing in your future" (J.E.B.). The authors thank H.-G. Sahl for providing *S. aureus* COL and nisin, Prof. K. Hiramatsu for providing *S. aureus* Mu50, L. Hamoen for providing *B. subtilis* 1981, A. Knüfer and C. Dilk for technical assistance with cytotoxicity testing, M. Strack for his help during RcPNA synthesis, and T. Bracht for sharing the Tecan plate reader.

■ REFERENCES

(1) Taubes, G. (2008) The bacteria fight back. *Science 321*, 360.

(2) Cafiso, V., Bertuccio, T., Spina, D., Purrello, S., Campanile, F., Di Pietro, C., Purrello, M., and Stefani, S. (2012) Modulating activity of vancomycin and daptomycin on the expression of autolysis cell-wall turnover and membrane charge genes in hVISA and VISA strains. *PLoS One 7*, e29573.

(3) Bertsche, U., Weidenmaier, C., Kuehner, D., Yang, S. J., Baur, S., Wanner, S., Francois, P., Schrenzel, J., Yeaman, M. R., and Bayer, A. S. (2011) Correlation of daptomycin resistance in a clinical *Staphylococcus aureus* strain with increased cell wall teichoic acid production and D-alanylation. *Antimicrob. Agents Chemother. 55*, 3922−3928.

(4) López, D., Vlamakis, H., Losick, R., and Kolter, R. (2009) Cannibalism enhances biofilm development in *Bacillus subtilis*. *Mol. Microbiol. 74*, 609−618.

(5) Rose, W. E., Fallon, M., Moran, J. J., and Vanderloo, J. P. (2012) Vancomycin tolerance in methicillin-resistant *Staphylococcus aureus*: influence of vancomycin, daptomycin, and telavancin on differential resistance gene expression. *Antimicrob. Agents Chemother. 56*, 4422−4427.

(6) Patra, M., Gasser, G., Bobukhov, D., Merz, K., Shtemenko, A. V., and Metzler-Nolte, N. (2012) Sequential insertion of three different organometallics into a versatile building block containing a PNA backbone. *Dalton Trans. 39*, 5617−5619.

(7) Bremner, J. B., Keller, P. A., Pyne, S. G., Boyle, T. P., Brkic, Z., David, D. M., Garas, A., Morgan, J., Robertson, M., Somphol, K., Miller, M. H., Howe, A. S., Ambrose, P., Bhavnani, S., Fritsche, T. R., Biedenbach, D. J., Jones, R. N., Buckheit, R. W., Jr., Watson, K. M., Baylis, D., Coates, J. A., Deadman, J., Jeevarajah, D., McCracken, A., and Rhodes, D. I. (2010) Binaphthyl-based dicationic peptoids with therapeutic potential. *Angew. Chem., Int. Ed. 49*, 537−40.

(8) Haug, B. E., Stense, W., Kalaaji, M., Rekdal, Ø., and Svendsen, J. S. (2008) Synthetic antimicrobial peptidomimetics with therapeutic potential. *J. Med. Chem. 51*, 4306−4314.

(9) Thaker, H. D., Som, A., Ayaz, F., Lui, D., Pan, W., Scott, R. W., Anguita, J., and Tew, G. N. (2011) Synthetic mimics of antimicrobial peptides with immunomodulatory responses. *J. Am. Chem. Soc. 11*, 11088−11091.

(10) Clinical and Laboratory Standards Institute. *Methods for Dilution Antimicrobial Susceptibility Tests for Bacteria That Grow Aerobically*, Approved Standard, 8th ed. Mo7-A8, Vol. *29* No. 2

(11) Wenzel, M., and Bandow, J. E. (2011) Proteomic signatures in antibiotic research. *Proteomics 11*, 3256−3268.

(12) Wenzel, M., Patra, M., Albrecht, D., Chen, Y. C., Nicolaou, K. C., Metzler-Nolte, N., and Bandow, J. E. (2011) Proteomic signature of fatty acid biosynthesis inhibition available for *in vivo* mechanism-of-action studies. *Antimicrob. Agents Chemother. 55*, 2590−2596.

(13) Wenzel, M., Kohl, B., Münch, D., Raatschen, N., Albada, H. B., Hamoen, L., Metzler-Nolte, N., Sahl, H.-G., and Bandow, J. E. (2012) Proteomic response of *Bacillus subtilis* to lantibiotics reflects differences in interaction with the cytoplasmic membrane. *Antimicrob. Agents Chemother. 56*, 5749−5757.

(14) Völker, U., Völker, A., and Haldenwang, W. G. (1996) Reactivation of the *Bacillus subtilis* anti-sigma B antagonist, RsbV, by stress- or starvation-induced phosphatase activities. *J. Bacteriol. 178*, 5456−5463.

(15) Hecker, M., and Völker, U. (2001) General stress response of *Bacillus subtilis* and other bacteria. *Adv. Microb. Physiol. 44*, 35−91.

(16) Meister, K., Niesel, J., Schatzschneider, U., Metzler-Nolte, N., Schmidt, D. A., and Havenith, M. (2010) Label-free imaging of metal-carbonyl complexes in live cells by Raman microspectroscopy. *Angew. Che. Int. Ed. 49*, 3310−3312.

(17) Strahl, H., and Hamoen, L. W. (2012) Membrane potential is important for bacterial cell division. *Proc. Natl. Acad. Sci. U.S.A. 27*, 12281−12286.

(18) Katsu, T., Kuroko, M., Morikawa, T., Sanchika, K., Fujita, Y., Yamamura, H., and Uda, M. (1989) Mechanism of membrane damage induced by the amphipathic peptides gramicidin S and melittin. *Biochim. Biophys. Acta 939*, 135−141.

(19) Schneider, T., Kruse, T., Wimmer, R., Wiedemann, I., Sass, V., Pag, U., Jansen, A., Nielsen, A. K., Mygind, P. H., Raventós, D. S., Neve, S., Ravn, B., Bonvin, A. M., De Maria, L., Andersen, A. S., Gammelgaard, L. K., Sahl, H.-G., and Kristensen, H. H. (2010) Plectasin, a fungal defensin, targets the bacterial cell wall precursor lipid II. *Science 328*, 1168−1172.

(20) Patra, M., Gasser, G., Pinto, A., Merz, K., Ott, I., Bandow, J. E., and Metzler-Nolte, N. (2009) Synthesis and biological evaluation of chromium bioorganometallics based on the antibiotic platensimycin lead structure. *ChemMedChem 4*, 1930−1938.

(21) Patra, M., Gasser, G., and Metzler-Nolte, N. (2012) Small organometallic compounds as antibacterial agents. *Dalton Trans. 41*, 6350−6358.

(22) Chantson, J. T., Verga Falzacappa, M. V., Crovella, S., and Metzler-Nolte, N. (2006) Solid-phase synthesis, characterization, and antibacterial activities of metallocene-peptide bioconjugates. *ChemMedChem 1*, 1268−1274.

(23) Chantson, J. T., Varga Falzacappa, M. V., Crovella, S., and Metzler-Nolte, M. (2005) Antibacterial activities of ferrocenoyl- and cobaltocenium-peptide bioconjugates. *J. Organomet. Chem. 690*, 4564−4574.

(24) Dubar, F., Egan, T. J., Pradines, B., Kuter, D., Ncokazi, K. K., Forge, D., Paul, J. F., Pierrot, C., Kalamou, H., Khalife, J., Buisine, E., Rogier, C., Vezin, H., Forfar, I., Slomianny, C., Trivelli, X., Kapishnikov, S., Leiserowitz, L., Dive, D., and Biot, C. (2011) The antimalarial ferroquine: role of the metal and intramolecular hydrogen bond in activity and resistance. *ACS Chem. Biol. 6*, 275−287.

(25) Dubar, F., Bohic, S., Dive, D., Guérardel, Y., Cloetens, P., Khalife, J., and Biot, C. (2012) Deciphering the Resistance-Counteracting Functions of Ferroquine in Plasmodium falciparum-Infected Erythrocytes. *ACS Med. Chem. Lett. 3*, 480−483.

(26) Biot, C., Nosten, F., Fraisse, L., Ter-Minassian, D., Khalife, J., and Dive, D. (2011) The antimalarial ferroquine: from bench to clinic. *Parasite 18*, 207−214.

(27) Brötz-Oesterhelt, H., and Sass, P. (2010) Postgenomic strategies in antibacterial drug discovery. *Future Microbiol. 5*, 1553−1579.

(28) Brötz-Oesterhelt, H., and Brunner, N. A. (2008) How many modes of action should an antibiotic have? *Curr. Opin. Pharmacol 8*, 564−573.

(29) Wadhwani, P., Afonin, S., Ieronimo, M., Buerck, J., and Ulrich, A. S. (2006) Optimized protocol for synthesis of cyclic gramicidin S: Starting amino acid is key to high yield. *J. Org. Chem. 71*, 55−61.

(30) Albada, H. B., Chiriac, A. I., Wenzel, M., Penkova, M., Bandow, J. E., Sahl, H. G., and Metzler-Nolte, N. (2012) Modulating the activity of short arginine-tryptophan containing antibacterial peptides with N-terminal metallocenoyl groups. *Beilstein J. Org. Chem. 8*, 1753−1764.

(31) Agnostopoulos, C., and Spizizen, J. (1961) Requirements for transformation in *Bacillus subtilis*. *J. Bacteriol. 81*, 741−746.

(32) Stülke, J., Hanschke, R., and Hecker, M. (1993) Temporal activation of betaglucanase synthesis in *Bacillus subtilis* is mediated by the GTP pool. *J. Gen. Microbiol. 139*, 2041−2045.

(33) Niesel, J., Pinto, A., Peindy N'Dongo, H. W., Merz, K., Ott, I., Gust, R., and Schatzschneider, U. (2008) Photoinduced CO release, cellular uptake and cytotoxicity of a tris(pyrazolyl)methane (tpm) manganese tricarbonyl complex. *Chem. Commun. 15*, 1798−1800.
(34) Matias, V. R., and Beveridge, T. J. (2008) Lipoteichoic acid is a major component of the *Bacillus subtilis* periplasm. *J. Bacteriol. 190*, 7414−7418.
(35) Matias, V. R., and Beveridge, T. J. (2005) Cryo-electron microscopy reveals native polymeric cell wall structure in *Bacillus subtilis* 168 and the existence of a periplasmic space. *Mol. Microbiol. 56*, 240−251.